RESEARCH ARTICLE | MAY 19 2025

Mechanism of nitrous oxide (HONO) formation in D-layer of ionosphere

Special Collection: Yijing Yan Festschrift

Hiroto Tachikawa

J. Chem. Phys. 162, 194307 (2025)
https://doi.org/10.1063/5.0271255

The Journal of Chemical Physics ARTICLE pubs.aip.org/aip/jcp

Mechanism of nitrous oxide (HONO) formation in D-layer of ionosphere

Cite as: J. Chem. Phys. 162, 194307 (2025); doi: 10.1063/5.0271255
Submitted: 16 March 2025 • Accepted: 1 May 2025 •
Published Online: 19 May 2025

Hiroto Tachikawa[a)]

AFFILIATIONS

Division of Applied Chemistry, Faculty of Engineering, Hokkaido University, Kita-ku, Sapporo 060-8628, Japan

Note: This paper is part of the Special Topic, Yijing Yan Festschrift.
[a)]**Author to whom correspondence should be addressed:** hiroto@eng.hokudai.ac.jp

ABSTRACT

Nitrous oxide (HONO) is an active oxidant and a major source of hydroxyl radicals in the D-layer of the ionosphere (60–90 km above the Earth's surface). However, the mechanism underlying the formation of HONO remains unclear. To elucidate the mechanism of HONO formation, sequential (stepwise) reactions of H_2O with NO^+ were investigated using direct *ab initio* molecular dynamics calculations. The target reactions were $NO^+(H_2O) + H_2O$ and $NO^+(H_2O)_2 + H_2O$, i.e., $NO^+(H_2O)_{n-1} + H_2O \rightarrow HONO{-}H^+(H_2O)_{n-1}$ (HONO product) (n = 2–5). In the case of n = 2, only the solvation of NO^+ by H_2O was found: $NO^+(H_2O) + H_2O \rightarrow NO^+(H_2O)_n$ (solvation product) (n = 2). HONO was obtained as the product at n = 3, although the reaction efficiency was low. The HONO product was efficiently formed when n = 4–5. The mechanism of HONO formation and the role of H_2O in the reactions are discussed based on theoretical analysis.

I. INTRODUCTION

Nitrous oxide (HONO) is an active oxidant and a major source of hydroxyl radicals (OH) in the atmosphere.[1,2] OH radicals generated from HONO are atmospheric purifying agents. HONO readily dissociates under sunlight to form OH and nitric oxide (NO) via the following reactions:[3,4]

$$HONO + h\nu \rightarrow NO + OH. \quad (1)$$

The photolysis of HONO contributes to more than 50% of the atmospheric OH radicals, which strongly affects the oxidation capacity of the atmosphere.[5–8]

It has been postulated that NO^+ reacts with H_2O to generate HONO in the D-layer of the ionosphere (60–90 km above the Earth's surface).[9–12] NO is ionized by ultraviolet rays. The resultant NO^+ can react with water molecules and clusters. Despite the importance of HONO, its mechanism of formation remains a long-standing puzzle.

The following three reaction models were considered for HONO formation (a schematic of the reaction model is shown in Fig. 1). In the first reaction model, NO^+ reacts with water clusters $(H_2O)_n$: the reaction path is expressed as **1** → **2** → **3** → **4** in Fig. 1.[13] This model is a collision reaction of NO^+ with $(H_2O)_n$. A previous study showed that HONO formation occurs at n = 4; the reaction is expressed as

$$NO^+ + (H_2O)_n \rightarrow HONO{-}H^+(H_2O)_{n-1} \quad \text{(reaction model 1)},$$

$$NO^+ + (H_2O)_n \rightarrow HONO + H^+(H_2O)_{n-1}.$$

The dissociation products were found for n = 4.

In the second reaction model, the reaction was caused by photoirradiation of the $NO(H_2O)_n$ clusters. This is an intracluster reaction within $NO^+(H_2O)_n$ caused by ionization of a neutral $NO(H_2O)_n$ cluster. The reaction path is expressed as: **6** → **7** → **2**→ **3** → **4** in Fig. 1,[14]

$$NO(H_2O)_n + h\nu \rightarrow \left[NO^+(H_2O)_n\right]_{ver} + e^-$$

$$\left[NO^+(H_2O)_n\right]_{ver} \rightarrow HONO{-}H^+(H_2O)_{n-1} \quad \text{(reation model 2)}.$$

$[M^+]_{ver}$ indicates the M^+ cluster at the vertical ionization point of the neutral cluster M. Upon photoionization of the neutral cluster, $NO^+(H_2O)_n$ is formed vertically. NO^+ attacks water molecules within the cluster, and HONO is produced after proton transfer

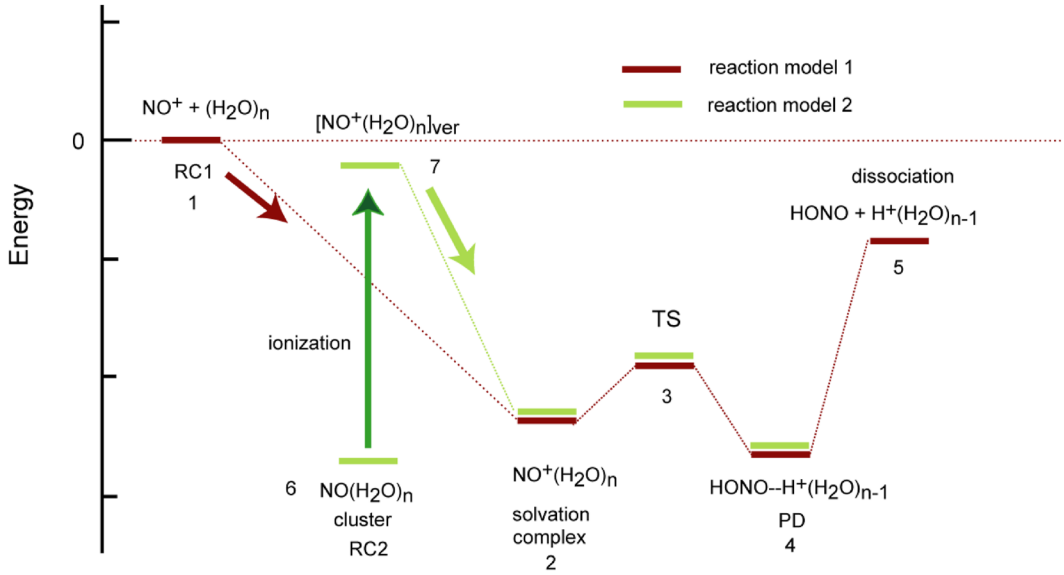

FIG. 1. Schematic energy diagram for reaction models 1 and 2 based on previous studies. Reaction model 1 indicates bi-molecular collision reaction, collision of NO^+ with water clusters $(H_2O)_n$, while reaction model 2 indicates ionization-induced reaction of $NO(H_2O)_n$ clusters. Both reaction models give the HONO product.

(PT). A previous theoretical study has shown that HONO formation occurs at $n = 4$.[14]

In the third reaction model, H_2O collides with NO^+ via the following stepwise mechanism:

$$NO^+ + H_2O \rightarrow NO^+(H_2O),$$

$$NO^+(H_2O) + H_2O \rightarrow NO^+(H_2O)_2,$$

$$NO^+(H_2O)_2 + H_2O \rightarrow NO^+(H_2O)_3 \quad \text{(reaction model 3)}.$$

That is,

$NO^+(H_2O)_{n-1} + H_2O \rightarrow NO^+(H_2O)_n \rightarrow$ product (sequential step-wise H_2O addition: reaction model 3).[15]

In this study, sequential (stepwise) reactions of H_2O with NO^+ (reaction model 3) were investigated using the direct *ab initio* molecular dynamics (AIMD) method in order to elucidate the mechanism of HONO formation in the D-layer of the ionosphere.

The reactions of NO^+–H_2O systems have been extensively studied by several researchers. Choi *et al.* used vibrational predissociation spectroscopy to observe the infrared spectra of mass-selected clusters of $NO^+(H_2O)_n$ for $n = 1$–5.[16] In small clusters ($n = 1$–3), the $NO^+(H_2O)_n$ complexes (solvation state) were the only ionic species. For the $n = 4$ clusters, the rearrangement reaction, $NO^+(H_2O)_4 \rightarrow HONO$–$H^+(H_2O)_3$, was observed after excitation of $NO^+(H_2O)_4$ with infrared (IR) photons; the reaction is expressed as: **2** → **3** → **4** in Fig. 1.

Angel and Stace experimentally investigated the formation of HONO using a double-focusing mass spectrometer.[15,17] In their experiment, $NO^+(H_2O)_n$ ($n = 2$–9) ions were mass-selected using a magnetic sector, and their unimolecular decay patterns were monitored in the field-free region of the mass spectrometer. They observed the formation of HONO in the presence of $NO^+(H_2O)_m + H_2O$ ($m = 3$ and 4).

Relph *et al.* observed the vibrational predissociation spectra of $NO^+(H_2O)_n$ ($n = 1$–4).[18] They found that HONO production started at $n = 4$ and proceeded via the intracluster conversion of $NO^+(H_2O)_n$. However, Eyet *et al.* investigated the thermal conversion of $NO^+(H_2O)_{3-4}$ to H_3O^+ at 150–400 K. They suggested that $NO^+(H_2O)_4$ is converted into HONO above 150 K.[19]

The structure and energetics of the $NO^+(H_2O)_n$ system were determined using an *ab initio* method. Ye and Cheng determined the hydration energies of NO^+ (with water molecules) to be 1.31 ($n = 1$), 0.87 ($n = 2$), and 0.77 eV ($n = 3$).[20] At the MP2/aug-cc-pVTZ level of theory, Asada *et al.* investigated the intracluster conversion reaction and energies for the formation of HONO and hydrated H_3O^+ ions from $NO^+(H_2O)_n$.[21] They suggested that HONO was obtained at $n = 4$ and 5 through an intracluster isomerization reaction, $NO^+(H_2O)_n \rightarrow HONO$–$H_3O^+(H_2O)_{n-2}$. He *et al.* investigated the thermal conversion using *ab initio* molecular dynamics (AIMD).[22] The calculations were performed at ionospheric temperature (200–220 K), indicating the following thermal conversion and thermal activation, respectively:

$$NO^+(H_2O)_4 \rightarrow HONO\text{–}H^+(H_2O)_3,$$

$$NO^+(H_2O)_5 \rightarrow HONO\text{–}H^+(H_2O)_4.$$

Sharma *et al.* reported that protonated water clusters are formed when a water molecule collides with a $NO^+(H_2O)_4$ cluster.[23] This reaction can be expressed as

$$NO^+(H_2O) + H_2O \rightarrow HONO + H^+(H_2O)_4. \quad (2)$$

In our previous studies,[13,14] the bi-molecular collision reaction[13] and ionization-induced reactions were investigated using direct AIMD (n = 1–7), as indicated in the following:[14]

$$NO^+(H_2O)_n \rightarrow HONO + H^+(H_2O)_{n-1} \quad (\text{bi-molecular collision (reaction model 1)}),$$

$$NO^+(H_2O)_n + h\nu \rightarrow HONO + H^+(H_2O)_{n-1} \quad (\text{ionization-induced reaction (reaction model 2)}).$$

In reaction model 1, the HONO formation channel opens from n = 3. However, the efficiency of HONO formation was significantly lower for n = 3 (0.38) in comparison to that of larger clusters with n = 4–7 (0.8–1.0), where the HONO formation channel became the main channel.[13] In reaction model 2, HONO was partially dissociated from the $HONO–H^+(H_2O)_{n-1}$ complex: $NO^+ + (H_2O)_n \rightarrow HONO–H^+(H_2O)_{n-1} \rightarrow HONO + H^+(H_2O)_{n-1}$.[14]

Thus, the intracluster arrangement and bimolecular- and ionization-induced reactions were thoroughly investigated using experiments and theoretical calculations to elucidate the formation of HONO. However, information regarding the sequential H_2O-addition reactions is lacking. In this study, the sequential reactions were investigated using the direct AIMD method[24–26] to shed light on the mechanism of HONO formation in the D-layer of the ionosphere. The target reaction is expressed as follows:

$$NO^+(H_2O)_n + H_2O \rightarrow \text{product} \quad (\text{reaction model 3}).$$

In this study, reaction model 3 was investigated using direct AIMD calculations to determine the possibility of atmospheric HONO formation.

II. COMPUTATIONAL DETAILS

A. *Ab initio* calculations

The geometries of the reactant clusters, $NO^+(H_2O)_n$ (n = 1–5), were fully optimized using CAM-B3LYP/6-311++G(d,p).[27] The second-order perturbation Møller–Plesset (MP2) method with the 6-311++G(d,p) basis set was also used.[28,29] The atomic and molecular charges were calculated using the natural population analysis (NPA) approach.[30] Standard Gaussian 09 and 16 program packages were used for all static *ab initio* calculations.[31,32]

B. Direct AIMD calculations

First, the structures of $NO^+(H_2O)_n$ and H_2O were separately optimized at the CAM-B3LYP/6-311++G(d,p) level. Thereafter, H_2O was randomly placed around $NO^+(H_2O)_n$. The distances of H_2O from $NO^+(H_2O)_n$ were set to larger than 6.0 Å (R = 6.0–7.0 Å). The trajectory calculation started from the geometries of the $NO^+(H_2O)_n–H_2O$ system under the zero collision energy condition: namely, the initial collision energy was set to zero for all trajectories (E_{coll} = 0.0 kcal/mol at time zero). A total of 20–50 trajectories was obtained from the geometries generated for each cluster size (n).

The initial vibrational and rotational temperatures, momentum vectors, and excess energy of $NO^+(H_2O)_n–H_2O$ were set to zero (0 fs). The maximum simulation time was 2.0 ps, and the time step was 0.01 fs. The velocity Verlet algorithm was used to solve the motion equations of the system. The deviation in the total energy was less than 0.01 kcal/mol. Direct AIMD calculations were performed using codes developed by the authors.[24–26]

Figure 2 shows a schematic of the collision sites of H_2O(W0) around $NO^+(H_2O)_n$ (n = 3 and 4). Regions I, II, III, and IV were located at angles of θ = 0–90°, 90–180°, 180–270°, and 270–360°, respectively. H_2O(W0) was detected from an intermolecular distance of R = 6.0–7.0 Å (time zero), and the collision of H_2O(W0) with $NO^+(H_2O)_n$ occurs in these regions.

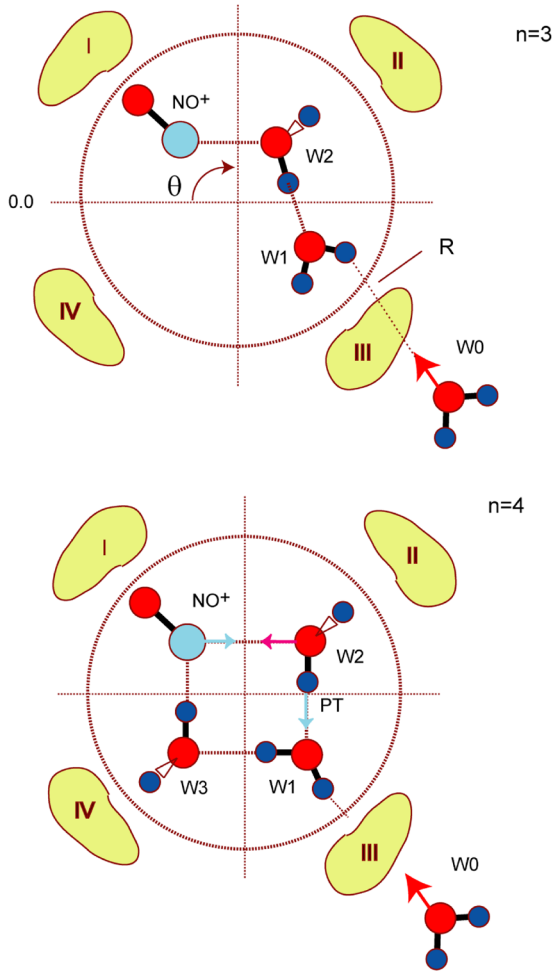

FIG. 2. Collision regions of H_2O around $NO^+(H_2O)_n$ at initial separation (time zero). Collision regions are classified into four regions in the present calculations. Region I: H_2O collides directly with NO^+. Regions II, III, and IV: H_2O collides with W2, W1, and W3, respectively.

III. RESULTS

A. Structures of $NO^+(H_2O)_n$ reactant molecules

First, the structures of the reactant molecules, $NO^+(H_2O)_n$ (n = 1–4) (ionic states), were optimized at the CAM-B3LYP/6-311++G(d,p) level. The obtained structures are shown in Fig. 3.

In the n = 1 cluster, the nitrogen atom of NO^+ binds to the oxygen atom of H_2O, with an intermolecular distance of 2.100 Å. For n = 2, one water molecule in the water dimer is bound to NO^+. The intermolecular distance between NO^+ and H_2O(W1) was 1.956 Å, corresponding to the N–O bond distance. A cyclic structure composed of NO^+ and $(H_2O)_3$ was obtained at n = 3. The intermolecular distances from NO^+ were 1.984 Å (W1) and 2.686 Å (W3), where W1 was significantly closer to NO^+. When n = 4, the fourth water molecule (W4) was bound to the cyclic structure of $NO^+(H_2O)_3$ (n = 3). W1 was strongly bound to NO^+ with a shorter bond length (2.035 vs 2.416 Å).

The structures of $NO^+(H_2O)_n$ (ionic state) were calculated at the MP2/6-311++G(d,p) level of theory. The results obtained at the MP2 level are shown in Fig. S1 in the supplementary material. Similar structures were observed.

B. Collision reaction of $NO^+(H_2O)_{n-1}$ + H_2O (n = 2)

In this section, the collision reaction of $NO^+(H_2O)$ + H_2O is investigated using direct AIMD calculations. First, the structures of $NO^+(H_2O)$ and H_2O were separately optimized at the CAM-B3LYP/6-311++G(d,p) level. Thereafter, H_2O was randomly placed around $NO^+(H_2O)$. The distances of H_2O from $NO^+(H_2O)$ were set to larger than 6.0 Å (R = 6.0–7.0 Å). The trajectory calculation started from these geometries with E_{coll} = 0.0 kcal/mol, and 30 trajectories were run. The calculations showed that only one solvation channel was obtained for n = 2, as shown in the following equation:

$$NO^+(H_2O) + H_2O \rightarrow NO^+(H_2O)_2 \qquad \text{(solvation channel)}.$$

A sample trajectory for n = 2 is shown in Fig. 4.

H_2O(W0) was located at R = 6.250 Å from $NO^+(H_2O)$, and the reaction started at time zero. In $NO^+(H_2O)$, the intermolecular distance between NO^+ and H_2O(W1) was $R1$ = 2.100 Å. The temporal evolution of the potential energy (PE) is shown in Fig. 4(b). The zero-PE level corresponds to the total energy of [$NO^+(H_2O)$ + H_2O]. At the start of the reaction, H_2O(W0) gradually approached $NO^+(H_2O)$, and the PE decreased. H_2O(W0) collided with H_2O(W1) of $NO^+(H_2O)$, where the PE was −15.1 kcal/mol at 495 fs. The intermolecular distances were R = 1.655 and $R1$ = 2.095 Å. At 554 fs, the O–H distance of H_2O(W1) was slightly elongated to $R2$ = 1.024 Å (vs 0.968 Å at time zero). However, proton transfer (PT) was not observed during these calculations. Finally, the solvation structure of $NO^+(H_2O)_2$ was obtained at 916 fs, where the potential energy was −15.5 kcal/mol.

The time-evolution of the potential energies of the five typical reaction trajectories is shown in Fig. S2. All trajectories provided a solvation channel.

C. Collision reaction of $NO^+(H_2O)_{n-1}$ + H_2O (n = 3)

In this section, the collision reaction of $NO^+(H_2O)_2$ with H_2O is investigated using direct AIMD calculations. First, the structures of $NO^+(H_2O)_2$ and H_2O were optimized separately at the CAM-B3LYP/6-311++G(d,p) level of theory. Thereafter, H_2O was

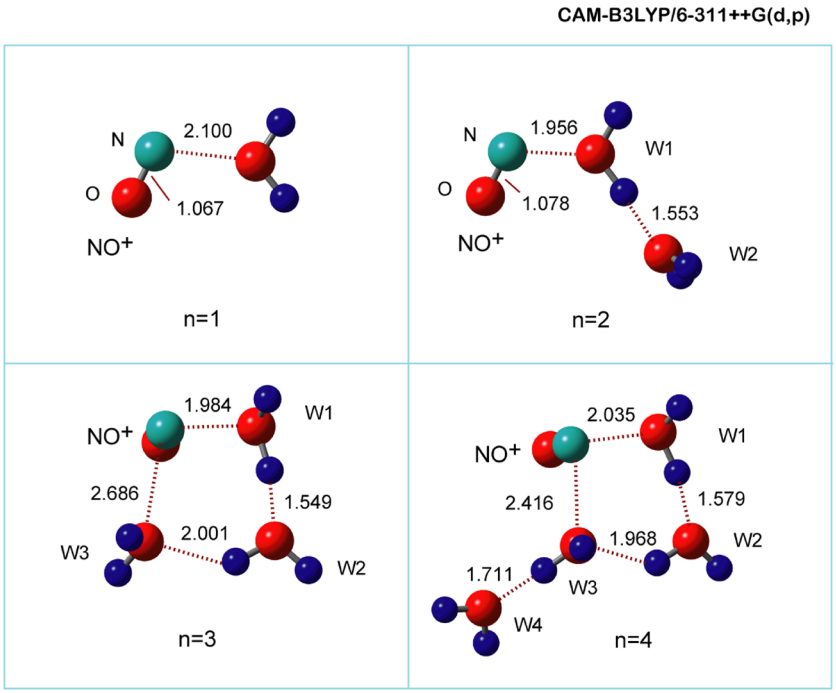

FIG. 3. Optimized structures of $NO^+(H_2O)_n$ (n = 1–4) (ionic state). The calculations were carried out at the *CAM-B3LYP*/6-311++G(d,p) level. Bond lengths are in Å.

randomly placed around $NO^+(H_2O)_2$. Forty trajectories were analyzed. The calculations showed that the two reaction channels (i.e., solvation and HONO product channels) were competitive at $n = 3$. The reactions can be expressed as follows:

$$NO^+(H_2O)_2 + H_2O \rightarrow NO^+(H_2O)_3 \quad \text{(solvation channel)},$$

$$NO^+(H_2O)_2 + H_2O \rightarrow HONO\text{–}H^+(H_2O)_2 \quad \text{(HONO product channel)}.$$

In the solvation channel, the product is $NO^+(H_2O)_3$, where NO^+ is solvated by H_2O, as well as the product with $n = 2$: $NO^+(H_2O) + H_2O \rightarrow NO^+(H_2O)_2$ (solvation in $n = 2$). The HONO product was identified as $n = 3$. However, the HONO product channel was minimal at $n = 3$. Almost all trajectories provided a solvation channel.

A sample trajectory for the HONO product channel (reactive channel) is shown in Fig. 5.

Snapshots and the PEs of $NO^+(H_2O)_2$–H_2O are shown in Figs. 5(a) and 5(b), respectively. In this sample trajectory, H_2O(W0) was placed at $R = 6.060$ Å from $NO^+(H_2O)_2$ (region III), and the reaction started at time zero. In $NO^+(H_2O)_2$, the intermolecular

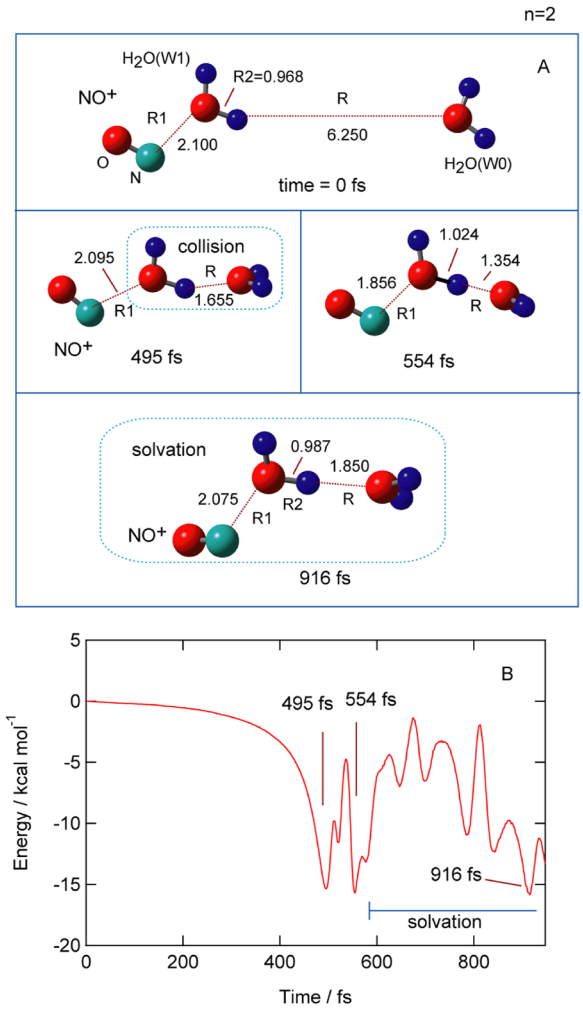

FIG. 4. (a) Snapshots and (b) time-evolution of potential energy (PE) for $NO^+(H_2O)$ + H_2O ($n = 2$) reaction system. Direct AIMD calculation was performed at the CAM-B3LYP/6-311++G(d,p) level. The CAM-B3LYP/6-311++G(d,p)-optimized geometries were used as the initial geometries of $NO^+(H_2O)$ + H_2O at time zero. Bond lengths are in Å.

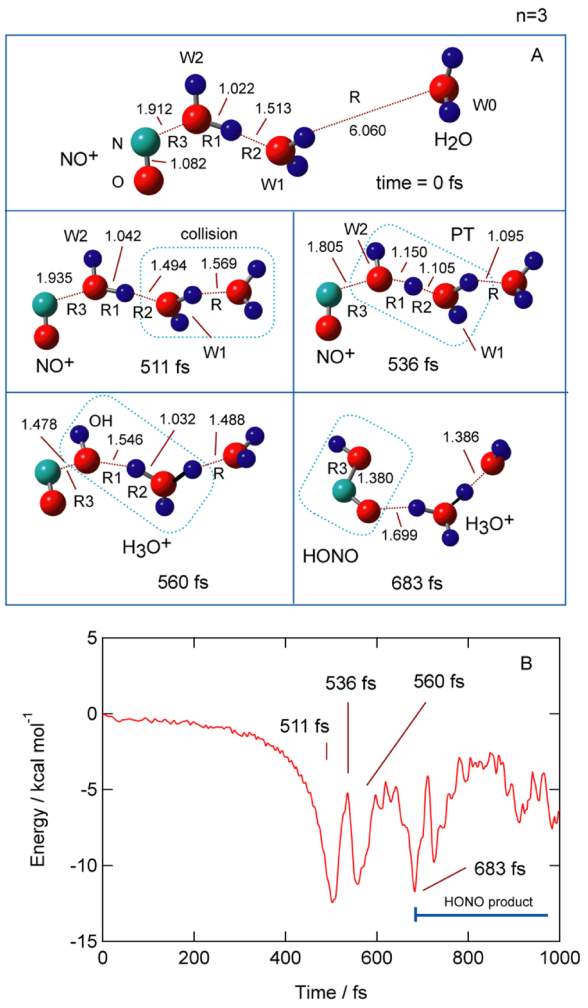

FIG. 5. (a) Snapshots and (b) time-evolution of PE in the $NO^+(H_2O)_2$ + H_2O ($n = 3$) reaction system. Direct AIMD calculation was performed at the CAM-B3LYP/6-311++G(d,p) level. The CAM-B3LYP/6-311++G(d,p)-optimized geometries were used as the initial geometries of $NO^+(H_2O)_2$ + H_2O at time zero. Bond lengths are in Å.

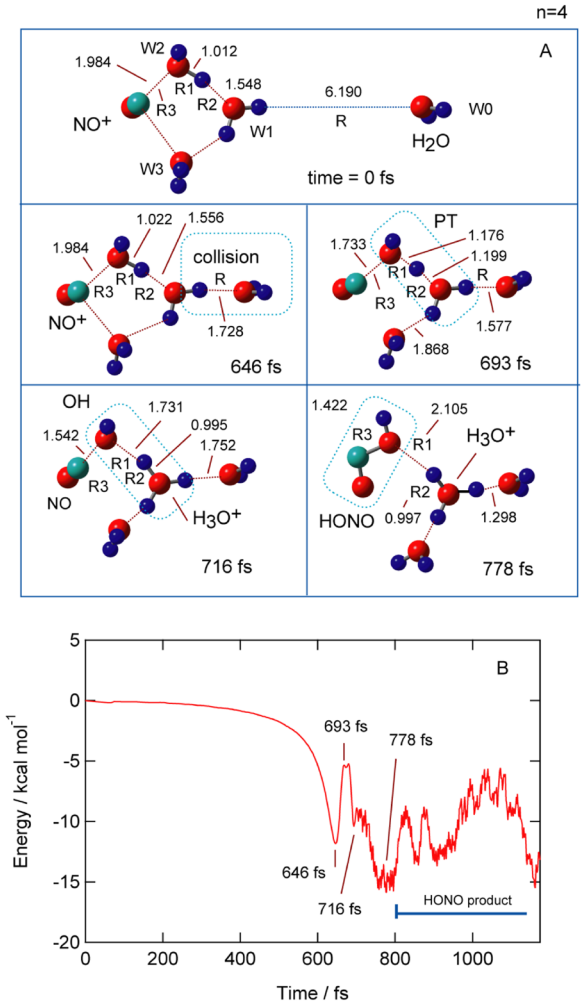

FIG. 6. (a) Snapshots and (b) time-evolution of PE in the $NO^+(H_2O)_3 + H_2O$ (n = 4) reaction system. Direct AIMD calculation was performed at the CAM-B3LYP/6-311++G(d,p) level. The CAM-B3LYP/6-311++G(d,p)-optimized geometries were used as the initial geometries of $NO^+(H_2O)_3 + H_2O$ at time zero. Bond lengths are in Å.

distance between H_2O(W1) and H_2O(W2) was $R2$ = 1.513 Å and the NO^+–H_2O(W2) distance was $R3$ = 1.912 Å at time zero.

At the start of the calculations, the PE of the reaction system [Fig. 5(b)] gradually decreases as H_2O approaches $NO^+(H_2O)_2$ (0–400 fs). After 400 fs, the energy suddenly decreases and reaches its lowest point at 511 fs. Here, H_2O(W0) collided with $NO^+(H_2O)_2$: the distance of H_2O(W0) from W1 was R = 1.569 Å. The geometrical parameters of $NO^+(H_2O)_2$ were $R1$ = 1.042, $R2$ = 1.494, and $R3$ = 1.935 Å, indicating that the original structure of $NO^+(H_2O)_2$ was retained after 511 fs.

After the collision, PT occurs from W2 to W1. At 536 fs, the proton of W2 was located at the midpoint between W1 and W2 (i.e., $R1$ = 1.150 and $R2$ = 1.105 Å). At 560 fs, the protons of W2 were fully transferred to W1, and H_3O^+ formed on W1. W2 was converted into OH radicals after PT. H_3O^+ was solvated with H_2O(W3). The generated OH radicals were attached to NO, and HONO was immediately formed at 683 fs. The PE was −11.0 kcal/mol. The final product was HONO–$H_3O^+(H_2O)$ (HONO product) in the reactive trajectories (n = 3). The time-evolution of the PEs for the five typical reactive trajectories is shown in Fig. S3. All trajectories exhibited similar tendencies. Almost all trajectories from regions I, II, and IV provided solvation channels.

D. Collision reaction of $NO^+(H_2O)_{n-1} + H_2O$ (n = 4)

This section presents the results for the $NO^+(H_2O)_3 + H_2O$ reaction. Figure 6 shows the time-evolution of the snapshots and PE of the $[NO(H_2O)_4]^+$ system in the reactive trajectory for n = 4.

At time zero, H_2O(W0) was located at R = 6.190 Å from W1 (region III). The collision energy of H_2O(W0) was set to zero (E_{coll} = 0 kcal/mol), and the optimized structures were used at time zero. The geometrical parameters of $NO^+(H_2O)_3$ were $R1$ = 1.012, $R2$ = 1.548, and $R3$ = 1.984 Å at time zero. After starting the trajectory, H_2O(W0) gradually approached and collided with H_2O(W2) at 646 fs (R = 1.728 Å). The original structure of $NO^+(H_2O)_3$ was retained at 646 fs. The PE decreased gradually with increasing time (0–400 fs): 0.0 kcal/mol at time = 0 fs, −1.0 kcal/mol at time = 400 fs, and −12.5 kcal/mol at 646 fs. After the collision, the PE suddenly increased to −5.2 kcal/mol at 693 fs. The structure of $NO^+(H_2O)_3$ changed significantly; the proton of W2 was transferred to W1, with $R1$ = 1.176 and $R2$ = 1.199 Å, suggesting that the proton was located at the midpoint between W1 and W2. The PT was completed at 716 fs, and H_3O^+ and OH radicals were formed ($R1$ = 1.731 and $R2$ = 0.995, respectively). The energy was −10.0 kcal/mol. After PT, the OH radicals rapidly attached to NO, and HONO was formed at 778 fs. The energy decreased to −16.0 kcal/mol (778 fs). The final product was HONO–$H^+(H_2O)_3$ (HONO product).

A total of 50 trajectories were executed for n = 4. Almost all the trajectories (from Region III) yielded reactive HONO products at n = 4. The reactions in the main channel are as follows:

$$NO^+(H_2O)_3 + H_2O \rightarrow \text{HONO–}H^+(H_2O)_3 \qquad \text{(HONO product channel)}.$$

The time-evolution of the PEs for the five typical reactive trajectories is shown in Fig. S4 (supplementary material). All trajectories exhibited similar tendencies. Almost all trajectories from regions I, II, and IV provided solvation channels.

The trajectories started from the top and bottom positions of the molecular plane of $NO^+(H_2O)_3$. The results are shown in Fig. S5. All calculations yielded nonreactive trajectories: solvation and dissociation channels. The dissociation is expressed as $NO^+(H_2O)_3$

+ $H_2O \rightarrow NO^+(H_2O)_3 + H_2O$ (dissociation) because the direction of the dipole moment of $NO^+(H_2O)_3$ is located on the molecular plane.

E. Collision reaction of $NO^+(H_2O)_{n-1} + H_2O$ (n = 5)

Similar calculations were performed for n = 5. The results are shown in Figs. S5 and S7 (supplementary material). Almost all trajectories from region III yielded the reactive HONO product at n = 5. The reactions in the main channel are as follows.

$$NO^+(H_2O)_4 + H_2O \rightarrow HONO\text{–}H^+(H_2O)_4.$$

The results of the trajectory calculations are summarized in Table S1 (supplementary material).

F. Energy diagram

The present dynamic calculations indicate that the HONO product was obtained from n = 3. HONO was not formed at n = 1 or 2. In this section, the energetics of $NO^+(H_2O)_n$ are surveyed based on static DFT calculations. A schematic of the NO^+–H_2O system is shown in Fig. 7.

Each solvation state has a corresponding zero-energy level, i.e., $NO^+(H_2O)_n$. In the n = 2 cluster, the energy levels of the reactant (RC) and HONO product states were 21.2 and 11.8 kcal/mol higher than that of the solvation state, respectively. In contrast, the energy of the HONO product was +0.5 kcal/mol lower than that of the solvation state for n = 3, suggesting that the reaction from the solvation to HONO product states (solvation → PD) is exothermic for n = 3. The exothermic energy further increased at n = 4 (6.9 kcal/mol) because the proton affinity of $(H_2O)_n$ increased with the cluster size (n), as shown in Fig. S8 (supplementary material). Therefore, the HONO product channel opens at n = 3. HONO formation proceeded more efficiently at n = 4–5. In addition, the energy level of the dissociated state of HONO (6.3 kcal/mol) was lower than that of the RC state (15.8 kcal/mol) for n = 4. Hence, isolated HONO is generated from n = 4. This is in good agreement with experimental results.[15,17] The exothermic energy increased further for the n = 5 clusters (15.2 kcal/mol).

G. Effects of DFT-functional on reaction mechanism

The direct AIMD calculations described in the previous sections were performed using the CAM-B3LYP functional. The effects of the functional (wB97XD) on the reaction mechanism are discussed in this section. The results for n = 2–5 are shown in Figs. S9–S12, respectively. Direct AIMD calculations at the wB97XD/6-311++G(d,p) level indicated that only the solvation channel product $NO^+(H_2O)_2$ was obtained at n = 2. In contrast, the HONO product opened at n = 3. HONO products were easily formed at n = 4 and n = 5. These results agree well with those obtained using the CAM-B3LYP-functional. Therefore, it can be concluded that the effects of functional groups on the reaction mechanism are exceedingly small.

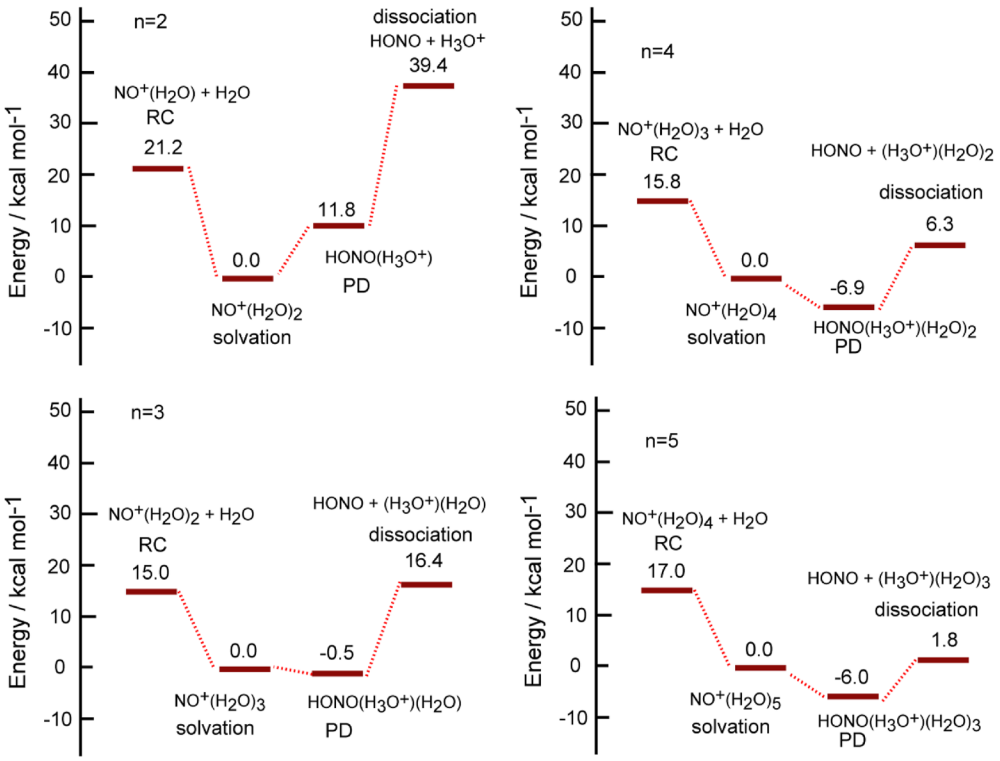

FIG. 7. Energy diagram of the $NO^+(H_2O)_{n-1} + H_2O$ (n = 2–5) reaction system. The calculations were performed at the CAM-B3LYP level with the 6-311++G(d,p) basis set. The values denote relative energies (in kcal/mol) calculated at the CAM-B3LYP/6-311++G(d,p) level.

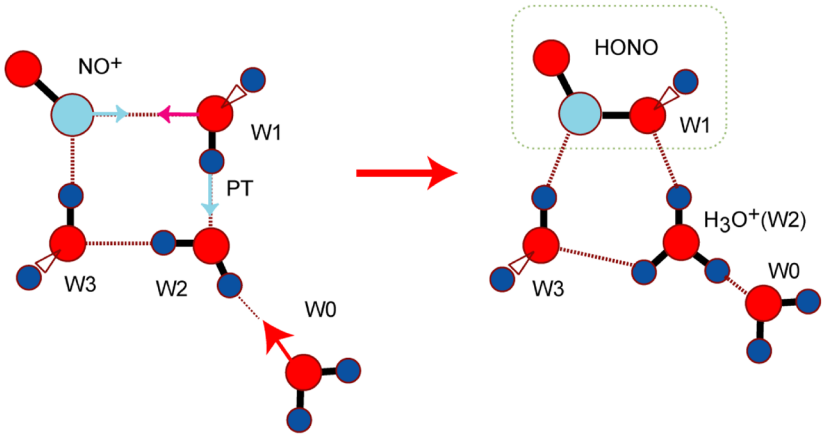

FIG. 8. Roles of H_2O in the formation of HONO in the reaction involving $NO^+(H_2O)_3 + H_2O$ ($n = 4$). PT denotes the proton transfer process.

IV. DISCUSSION

A. Role of H_2O in HONO formation

Figure 8 shows a schematic of the roles of water molecules in the reaction.

The roles of each water molecule are discussed in this section. Collisions in region III were also considered. H_2O(W0) is the water molecule that collides with $NO^+(H_2O)_n$. This water molecule provides energy (hydrogen bonding energy) to $NO^+(H_2O)_n$ after colliding with H_2O(W2) and increases the proton affinity of H_2O(W2). H_2O(W1) provides a proton to W2 along the hydrogen bond and generates OH radicals after proton transfer to W2. Subsequently, the OH radicals attack NO to form HONO. Proton-accepting H_2O(W2) forms H_3O^+. H_2O(W3) stabilizes H_3O^+(W2). Thus, all water molecules play a key role in the reactions for $n = 3$ and 4. However, the surface area of the reactive sites (Region III) decreased with increasing cluster size. Therefore, the reactivity peaked at an appropriate cluster size.

B. Reaction mechanism

In this section, the detailed reaction mechanism is discussed based on the calculated results. The reactions are expressed as follows:

$$NO^+(H_2O)_3 + H_2O(W0) \rightarrow NO^+(H_2O{-}H_2O){-}H_2O(W0) \quad \text{(collision)}$$

$$\rightarrow [NO{-}H_2O{-}H_2O]^+ {-}H_2O(W0) \quad \text{(charge delocalization and PT)}$$

$$\rightarrow NO(OH{-}H_3O^+){-}H_2O(W0)$$

$$HONO{-}(H_3O^+){-}H_2O(W0) \quad \text{(OH attact and solvation).}$$

H_2O(W0) collides with $NO^+(H_2O)_2$ in the first stage of the reaction (collision). Thereafter, charge delocalization between NO^+ and $(H_2O{-}H_2O)$ takes place within the cluster: $NO^+(H_2O{-}H_2O) \rightarrow [NO{-}H_2O{-}H_2O]^+$ (charge delocalization). The ensuing process is PT within the water-dimer cation $(H_2O{-}H_2O)^+$, represented as $(H_2O{-}H_2O)^+ \rightarrow (OH{-}H_3O^+)$, where an OH radical is formed within the water-dimer cation. The OH radical immediately attacks the NO radical, resulting in the spontaneous formation of HONO via radical–radical recombination (OH attack). Charge delocalization and PT occur simultaneously, as shown in Fig. S13. The H_3O^+ ions are stabilized by H_2O(W0) (solvation).

As the number of H_2O molecules in the $NO^+(H_2O)_n$ cluster increased, the solvation energy of H_3O^+ increased. Hence, the reaction efficiency also increased with an increasing number of water molecules (n). However, the surface area of the reactive sites (region III) decreased with increasing cluster size. Therefore, the reactivity peaked at an appropriate cluster size. This reaction mechanism explains the formation of HONO.

C. Reaction model

The reaction model for the sequential addition of H_2O to the NO^+ system is presented in this section. Figure 9 shows a schematic of the potential energy curve for the sequential H_2O addition.

The energy level at $n = 1$ indicates the solvation state of $NO^+(H_2O)$. The addition of H_2O to $NO^+(H_2O)$ results in the solvation state of $NO^+(H_2O)_2$ at $n = 2$. The energy level of the HONO product state at $n = 2$ was higher than that of the solvation state. In

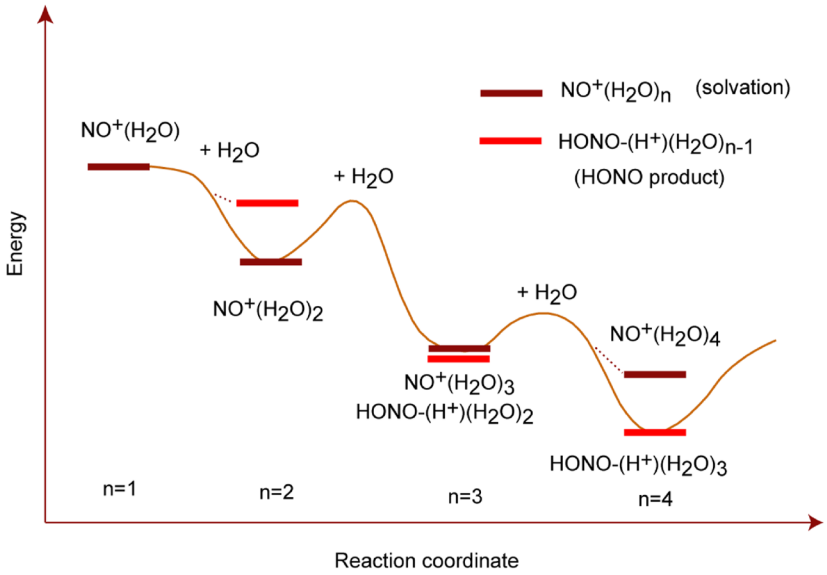

FIG. 9. Schematic of PE curves for the sequential addition of H_2O to $NO^+(H_2O)_{n-1}$. The red and green curves indicate reaction pathways for solvation and HONO product channels, respectively.

contrast, the energy of the HONO product state was comparable to that of the solvation state at $n = 3$. Hence, the HONO product channel opens from $n = 3$, although the HONO product is minor. At $n = 4$, the major channel changed to the HONO product state because the energy level of the HONO product state was lower than that of the solvation state. Therefore, the relative energies of the solvation and HONO product states dominate the reaction mechanism.

V. CONCLUSION

Understanding the atmospheric formation of nitrous acid (HONO) is a long-standing problem. In this study, the reactions involved in the formation of HONO were investigated using direct AIMD calculations. Sequential (stepwise) addition of H_2O to NO^+ was proposed. The following main channels were identified from direct AIMD calculations:

$$NO^+(H_2O) + H_2O \rightarrow NO^+(H_2O)_2 \quad \text{(solvation state: } n = 2\text{)},$$

$$NO^+(H_2O)_2 + H_2O \rightarrow NO^+(H_2O)_3 \quad \text{(solvation state: } n = 3\text{)},$$

$$NO^+(H_2O)_3 + H_2O \rightarrow HONO\text{–}H^+(H_2O)_3 \quad \text{(HONO product state: } n = 4\text{)},$$

$$NO^+(H_2O)_4 + H_2O \rightarrow HONO\text{–}H^+(H_2O)_4 \quad \text{(HONO product state: } n = 5\text{)}.$$

The calculations clearly suggest that the sequential reaction easily produces HONO without any collision energy for $n = 4$.

In the D-layer of the ionosphere (height of 60–90 km), NO is ionized by x rays and UV rays (1216 Å) from the sun. Hence, the sequential stepwise addition of H_2O to NO^+ occurs easily. This study suggests that HONO can be formed via sequential (stepwise) reactions. In contrast, the densities of water and $NO(H_2O)_n$ clusters in the D-layer are low. Hence, the probability of reaction model 3 is greater than those of reaction models 1 and 2. Model 3 represents the most favorable reaction.

SUPPLEMENTARY MATERIAL

The data supporting the findings of this study are available in the supplementary material. Optimized structures of $NO^+(H_2O)$ (n = 1–4), time-evolution of potential energy (PE) for $NO^+(H_2O) + H_2O$ (n = 2–5) reaction system, proton affinities of water clusters (n = 1–7), NPA charge of NO for $NO^+(H_2O)_{n-1} + H_2O$ (n = 4) reaction system, and the results of direct AIMD calculation performed at the wB97XD/6-311++G(d,p) level are provided in the supplementary material.

ACKNOWLEDGMENTS

The authors acknowledged partial support from JSPS KAKENHI (Grant Nos. 21H05415 and 21K04973).

AUTHOR DECLARATIONS

Conflict of Interest

The author has no conflicts to disclose.

Author Contributions

Hiroto Tachikawa: Investigation (equal).

DATA AVAILABILITY

The data that support the findings of this study are available within the article and its supplementary material.

REFERENCES

[1]T. Berndt, S. Richters, R. Kaethner, J. Voigtländer, F. Stratmann, M. Sipilä, M. Kulmala, and H. Herrmann, J. Phys. Chem. A **119**, 10336–10348 (2015).
[2]B. Feng, C. Sun, W. Zhao, and S. Zhang, Environ. Sci.: Processes Impacts **22**, 1554–1565 (2020).
[3]E. Praske, J. D. Crounse, K. H. Bates, T. Kurtén, H. G. Kjaergaard, and P. O. Wennberg, J. Phys. Chem. A **119**, 4562–4572 (2015).
[4]X. Huang, D. Wang, Q. Yang, Y. Peng, and J. Li, Appl. Catal., B **285**, 119835 (2021).
[5]J. Kleffmann *et al.*, "Daytime formation of nitrous acid: A major source of OH radicals in a forest," Geophys. Res. Lett. **32**, L05818, https://doi.org/10.1029/2005GL022524 (2005).
[6]Z. Tan *et al.*, "Wintertime photochemistry in Beijing: observations of RO_x radical concentrations in the North China Plain during the BEST-ONE campaign," Atmos. Chem. Phys. **18**, 12391–12411 (2018).
[7]G. Villena *et al.*, "Nitrous acid (HONO) during polar spring in barrow, Alaska: A net source of OH radicals?," J. Geophys. Res. **116**, D00R07, https://doi.org/10.1029/2011JD016643 (2011).
[8]M. Song, X. Zhao, P. Liu *et al.*, npj Clim. Atmos. Sci. **6**, 30 (2023).
[9]F. C. Fehsenfeld and E. E. Ferguson, J. Geophys. Res. **74**, 2217–2222, https://doi.org/10.1029/JA074I009P02217 (1969).
[10]A. Good, D. A. Durden, and P. Kebarle, J. Chem. Phys. **52**, 222–229 (1970).
[11]X. Zhang *et al.*, "Elucidating HONO formation mechanism and its essential contribution to OH during haze events," npj Clim. Atmos. Sci. **6**, 55 (2023).
[12]F. C. Fehsenfeld and E. E. Ferguson, "Origin of water cluster ions in the *D* region," J. Geophys. Res. **74**, 2217–2222, https://doi.org/10.1029/JA074i009p02217 (1969).
[13]H. Tachikawa, J. Phys. Chem. A **126**, 119–124 (2022).
[14]H. Tachikawa, "Intracluster reaction dynamics of $NO^+(H_2O)_n$," J. Chem. Phys. **161**, 094306 (2024).
[15]L. Angel and A. J. Stace, J. Chem. Phys. **109**, 1713–1715 (1998).
[16]J.-H. Choi, K. T. Kuwata, B.-M. Haas, Y. Cao, M. S. Johnson, and M. Okumura, J. Chem. Phys. **100**, 7153–7165 (1994).
[17]L. Angel and A. J. Stace, J. Phys. Chem. A **102**, 3037–3041 (1998).
[18]R. A. Relph *et al.*, "How the shape of an H-bonded network controls proton-coupled water activation in HONO formation," Science **327**, 308–312 (2010).
[19]N. Eyet, N. S. Shuman, A. A. Viggiano, J. Troe, R. A. Relph, R. P. Steele, and M. A. Johnson, J. Phys. Chem. A **115**, 7582–7590 (2011).
[20]L. Ye and H.-P. Cheng, J. Chem. Phys. **108**, 2015–2023 (1998).
[21]T. Asada, M. Nagaoka, and S. Koseki, Phys. Chem. Chem. Phys. **13**, 1590–1596 (2011).
[22]R. He *et al.*, "Resolving the HONO formation mechanism in the ionosphere via ab initio molecular dynamic simulations," Proc. Natl. Acad. Sci. U. S. A. **113**, 4629–4633 (2016).
[23]S. Sharma, T. G. Wright, and N. A. Besley, Phys. Chem. Chem. Phys. **20**, 25931–25938 (2018).
[24]H. Tachikawa and H. Kawabata, J. Phys. Chem. A **124**, 8421–8428 (2020).
[25]H. Tachikawa, "Mechanism of ionic dissociation of HCl in the smallest water clusters," Phys. Chem. Chem. Phys. **26**, 3623–3631 (2024).
[26]H. Tachikawa, "Reaction mechanism of an intracluster S_N2 reaction induced by electron capture," Phys. Chem. Chem. Phys. **24**, 3941–3950 (2022).
[27]T. Yanai, D. P. Tew, and N. C. Handy, Chem. Phys. Lett. **393**, 51–57 (2004).
[28]A. D. McLean and G. S. Chandler, J. Chem. Phys. **72**, 5639–5648 (1980).
[29]M. Head-Gordon and T. Head-Gordon, Chem. Phys. Lett. **220**, 122–128 (1994).
[30]A. E. Reed, R. B. Weinstock, and F. Weinhold, J. Chem. Phys. **83**, 735–746 (1985).
[31]M. J. Frisch, G. W. Trucks, H. B. Schlegel, G. E. Scuseria, M. A. Robb, J. R. Cheeseman, G. Scalmani, V. Barone, B. Mennucci, G. A. Petersson *et al.*, *Gaussian 09, Revision D.01*, Gaussian, Inc., Wallingford, CT, 2013.
[32]M. J. Frisch, G. W. Trucks, H. B. Schlegel, G. E. Scuseria, M. A. Robb, J. R. Cheeseman, G. Scalmani, V. Barone, G. A. Petersson *et al.*, *Gaussian 16, Revision A.03*, Gaussian, Inc., Wallingford, CT, 2016.